The prompt emission of GRB990712 with *BeppoSAX*: evidence of a transient X–ray emission feature

F. Frontera[1,2], L. Amati[2], M. Vietri [3], J.J.M. in 't Zand[4] E. Costa[5], M. Feroci[3], J. Heise[4], N. Masetti[2], L. Nicastro[6], M. Orlandini[2], E. Palazzi[2], E. Pian[2], L. Piro[5], P. Soffitta[5]

[1]Dipartimento di Fisica, Università di Ferrara, Via Paradiso 12, 44100 Ferrara, Italy

[2]Istituto Tecnologie e Studio Radiazioni Extraterrestri, CNR, Via Gobetti 101, 40129 Bologna, Italy

[3]Dipartimento di Fisica, Terza Università di Roma, via della Vasca Navale, 84, 00146 Roma

[4]Space Research Organization in the Netherlands, Sorbonnelaan 2, 3584 CA Utrecht, The Netherlands

[5]Istituto Astrofisica Spaziale, C.N.R., Via Fosso del Cavaliere, 00133 Roma, Italy

[6]Istituto Fisica Cosmica e Applicazioni all'Informatica, C.N.R., Via U. La Malfa 153, 90146 Palermo, Italy

arXiv:astro-ph/0102234v2 19 Mar 2001

ABSTRACT

We report on the prompt X– and γ–ray observations of GRB990712 with the *BeppoSAX* Gamma-Ray Burst Monitor and Wide Field Camera No. 2. Due to Sun constraints, we could not perform a follow-up observation with the *BeppoSAX* Narrow Field Instruments. The light curve of the prompt emission shows two pulses and a total duration of about 40 s in X-rays. In gamma–rays the event is even shorter. The 2–700 keV spectral emission with time shows a discontinuity in the peak energy E_p of the $EF(E)$ spectrum: E_p is above our energy passband during the first pulse and goes down to ~ 10 keV during the second pulse. Another peculiarity is noted in this event for the first time: the evidence of a 2 s duration emission feature during the tail of the first pulse. The feature is consistent with either a Gaussian profile with centroid energy of 4.5 keV or a blackbody spectrum with $kT_{bb} \sim 1.3$ keV. We discuss the possible origin of the feature. The most attractive possibility is that we are observing the thermal emission of a baryon-loaded expanding fireball, when it becomes optically thin.

Subject headings: gamma rays: bursts — gamma rays: observations — X–rays: general —shock waves

1. Introduction

Observations of cosmic Gamma-Ray Bursts (GRBs) with the *BeppoSAX* satellite are providing a key contribution to theories about their nature. Among the still unsettled questions, it is still not clear what are the mechanisms that produce the observed X–ray spectra and their evolution with time (see, e.g., Frontera et al. 2000) and what are the environments in which the GRBs occur. In the context of the internal shock model,

synchrotron radiation is generally expected to play an important role in the production of the observed GRB spectra (e.g., Tavani 1996), but Inverse Compton can also give a significant contribution to them (Ghisellini et al. 2000). Also blackbody emission from the photosphere of the fireball (Mészáros & Rees 2000) is expected to contribute to the GRB spectra, and inhomogeneities in the GRB outflow, made of dense highly ionized metal–rich material, could give rise to broad spectral features, mainly K-edges (Mèszàros and Rees 1998). Effects of photoelectric absorption and Compton scattering from the circumburst material can modify the intrinsic energy spectrum of the GRBs, with the introduction of absorption cut-offs and features, such as K-edges and emission lines (Mèszàros and Rees 1998; Böttcher et al. 1999), the presence of which has already been reported for some GRBs (Yoshida et al. 1999; Piro et al. 1999; Antonelli et al. 2000; Piro et al. 2000; Amati et al. 2000). The separation of the intrinsic and external components is of key importance for establishing both the GRB emission mechanisms and the properties of the GRB environment.

The Gamma Ray Burst Monitor (GRBM, 40–700 keV, Frontera et al. 1997), and the two Wide Field Cameras (WFC, 2–28 keV, Jager et al. 1997) on board *BeppoSAX* offer the opportunity to study the GRB energy spectra in the 2–700 keV energy band where the above components can be investigated (e.g., Frontera et al. 2000). GRB990712 was detected by the WFC No. 2 and the GRBM, showing in the 2–26 keV band the highest peak flux ever observed from a GRB with *BeppoSAX*. Its position was promptly distributed to the astronomical community (Frontera et al. 1999). Follow–up observations with the *BeppoSAX* Narrow Field Instruments were not possible due to Sun constraints. Observations were performed in the optical and radio bands. An optical transient (OT) with magnitude $R = 19.4 \pm 0.1$ was discovered about 3 hrs after the event (Bakos et al. 1999) and its redshift is now well determined ($z = 0.4331 \pm 0.0004$) (Vreeswijk et al. 2001).

2. Observations

GRB990712 was detected on July 12, 1999 starting on 16:43:02 UT (Frontera et al. 1999). Its position was determined with an error radius of $2'$ (99% confidence level) and was centered at $\alpha_{2000} = 22^{\mathrm{h}}31^{\mathrm{m}}50^{\mathrm{s}}$, $\delta_{2000} = -73°24'24''$ (Heise et al. 1999). Features and data available from GRBM and WFCs have already reported in several papers (e.g., Frontera et al. 2000). The effective area exposed to the GRB was ≈ 420 cm^2 in the 40–700 keV band and 37 cm^2 in the 2–26 keV energy band. The background in the WFC and GRBM energy bands was fairly stable during the event. The WFC spectra were extracted through the Iterative Removal Of Sources procedure (IROS, e.g. Jager et al. 1997) which implicitly subtracts the contribution of the background and of other point sources in the field of view. The count rate spectra were analyzed using the XSPEC v. 10 software package (Arnaud 1996). The quoted errors for the spectral parameters correspond to 90% confidence. Parameter values shown in brackets in Table 1 have been fixed while fitting.

3. Results

Figure 1 shows the time profile of GRB990712 in four energy bands after the background subtraction. In all bands the GRB shows a double–pulse structure, with an opposite behavior with energy of the first pulse with respect to the second: the peak flux of the first pulse increases with energy, while that of the second pulse decreases. The total duration of the event is about 20 s above 100 keV, but much longer (about 40 s) over the full 2–26 keV range. The spectral evolution of the event was studied by subdividing the GRB time profile into 8 adjacent time intervals and performing an analysis of the spectrum of each interval (see Fig. 1). We fit the spectra with either a power law (PL, $N(E) \propto E^{\alpha}$), a broken power–law (BKN–PL) or a smoothly broken power law (BL, Band et al. 1993), with photoelectric absorption (WABS model in XSPEC). We assumed the Galactic hydrogen

column density N_{H} ($= 4.52 \times 10^{20}\,\mathrm{cm}^{-2}$, Dickey & Lockman 1990) along the line of sight to the GRB. For the first three time slices the fit was also performed leaving N_{H} free to vary, but unfortunately N_{H} was not constrained by the data. The fit results with a PL and a BL are given in Table 1. The results obtained with the BKN–PL model were similar to those obtained with the BL model and are not reported in Table 1. The spectra of the time intervals A and B, that correspond to the rise of the first pulse of the GRB, and the spectrum of the interval D, that corresponds to the late tail of this pulse, are well fitted with a PL model. The BL model provides a good description of the spectra in the time intervals E and F, that correspond to the core of the second pulse, while the PL model again well describes the tail of the second pulse (intervals G and H). However neither of these models provides a good description of the C spectrum ($\chi^2/\nu = 16/6$ for a PL and $16/5$ for a BL). An excess with a significance level of about 3σ is evident around 4 keV. We investigated a possible instrumental origin of this anomaly with negative results. The WFC high-voltage, which is monitored every second, does not show any glitch in the interval C. Given the accuracy of the readout (which dominates over statistical noise) this excludes gain changes higher than 0.01%. As in other GRB detections, the WFC ratemeters all show the gamma-ray burst, even the ones that measure the illegal events, so we do not find any anomaly in this event. There are no dips or spikes of any sort, with a typical 3σ upper limit of 10% per second of measurement (for a count rate of 700 counts s^{-1}). There is one thermometer that shows a small change about 10 s before the burst, but all other measurements do not show anything out of the ordinary. The count excess in the GRB spectrum of the interval C is also clearly visible (see Figure 2) in the ratio between the C count spectrum and the Crab spectrum measured when this source was observed at an angular offset similar to that of GRB990712. For comparison, Figure 2 also shows the ratio with Crab of the spectra measured in the intervals B and D, that precede and follow C, respectively. As can be seen, in the interval B the greater hardness of the GRB spectrum

(photon index of ∼1.4, see Table 1) than that of Crab is apparent, while in the interval D the flatness of the Crab ratio is consistent with the similar slope of the GRB spectrum (see Table 1) with that of Crab. A slight hint of the 4 keV excess in the spectrum also appears in the interval B, but it is not statistically significant. We point out that the Crab ratio technique is adopted, to discover cyclotron lines in the spectra of X-ray pulsars (e.g., Dal Fiume et al. 2000).

The addition of a Gaussian function or a blackbody spectrum (BB) to a PL model provides a good fit ($\chi^2/\nu = 1.6/5$ and $\chi^2/\nu = 6.2/6$, respectively) of the C spectrum. The best fit parameters of both models are reported in Table 2. For a better determination of the Gaussian and BB parameters, the photon index α of the PL model was kept fixed in the fit to the best fit value, that is given by 1.34 ± 0.17 or 1.24 ± 0.20, depending on the model assumed for the feature, a Gaussian or a BB model, respectively. The count rate spectrum of the interval C along with the best fit curve of the PL plus a blackbody model is shown in the top panel of the Figure 3, while the ratio between the count spectrum and the best fit power-law alone is shown in the bottom panel. The excess counts to the PL model are apparent. The evolution of the logarithmic power per photon decade (the $EF(E)$ spectrum) with the time from the GRB onset is shown in Figure 3. The emission feature during the C interval is also apparent in this plot. The peak energy of the $EF(E)$ spectrum (see Table 1) is above our energy passband for the entire duration of the first pulse before suddenly becoming much lower (∼ 10 keV) from the beginning of the second pulse.

From the spectral fits we derived GRB fluence and peak flux. The γ–ray (40–700 keV) fluence of the burst is $S_\gamma = (6.5\pm0.3)\times10^{-6}$ erg cm^{-2}, while the corresponding value found in the 2–10 keV band is $S_X = (2.60\pm0.06)\times10^{-6}$ erg cm^{-2}, with a ratio $S_X/S_\gamma = 0.40\pm0.03$, which is one of the highest values found with *BeppoSAX* (Frontera et al. 2000). The 2–700 keV fluence is given by $S_\gamma = (1.10 \pm 0.03) \times 10^{-5}$ erg cm^{-2}. The γ–ray peak flux

is $P_\gamma = 4.1 \pm 0.3$ photons/cm^2 s corresponding to $(1.3 \pm 0.1) \times 10^{-6}$ erg cm^{-2} s^{-1}, while the corresponding 2–10 keV peak flux is $P_X = 41 \pm 4$ photons/cm^2 s, corresponding to $(3.3 \pm 0.3) \times 10^{-7}$ erg cm^{-2} s^{-1}.

4. Discussion

From the redshift value of the optical afterglow of GRB990712 ($z = 0.4331$, Vreeswijk et al. 2001) we can derive the X– plus γ–ray energy released in the main event. Assuming isotropic emission and a standard Friedman cosmology ($H_0 = 70$ km s^{-1} Mpc^{-1} and $q_0 = 0.5$), we get a 2–700 keV released energy of $E_{rel} = (5.9 \pm 0.2) \times 10^{51}$ erg. A sizeable fraction of this energy ($\sim 20\%$) is released between 2 and 10 keV. If we exclude the controversial case of GRB980425/SN1998bw (Galama et al. 1998; Kulkarni et al. 1998; Pian et al. 2000), GRB990712, in addition to showing the lowest redshift, is one of the least energetic events.

GRB990712 is marked by a peculiarity, which is noted here for the first time: the evidence of a broad emission feature at 4.4 keV, visible for 2 s, superposed on a power law continuum model. It can be described by either a Gaussian profile with a full width at half maximum of ~ 3 keV or a blackbody emission with $kT_{bb} = 1.3$ keV. If we assume the Gaussian description, its centroid energy corrected for redshift ($E_0 = 6.4 \pm 1.1$ keV) is consistent with the energy of both an iron K fluorescence line and a iron recombination line. The interpretation of the emission feature as an iron recombination line is tempting, yet it makes some stringent demands on models: in fact, it requires much mass to be present within a few light seconds of the burst site, and for this mass to be moving at Newtonian speeds. Vietri et al (2001) derive the expected rate of photons for a narrow line:

$$\dot{N}_{Fe} \approx \frac{4 \times 10^{52}}{T_7^{3/4}} \ s^{-1} \frac{M_{Fe}}{1 M_\odot} \frac{6 \times 10^{15} \ cm}{R} \tag{1}$$

where T_7 and R are the electron temperature (units of 10^7 K) and the external radius of the

line emitting medium, respectively, and M_{Fe} is the iron mass present in this medium. For a broad line, such as that in GRB990712, the above value is an understimate by a factor of a few at most. Assuming $T_7 = 1$, $R = 6 \times 10^{15}$ cm and $M_{\mathrm{Fe}} = 1 M_\odot$, comparison with Table 2 shows that Eq. 1 underestimates the observed line luminosity by four to five orders of magnitude; inserting $R = 10$ light seconds in the above equation yields the correct line luminosity, but for a total mass of iron of *at least* $M_{Fe} = 0.1 M_\odot$. Assuming a realistic iron relative abundance (at least 1% of the total mass, if what we are seeing is a type I SN, but more for any other hypothesis) shows that we must explain the presence of at least $10 M_\odot$ of matter, at radii of a few light seconds, with none of this obstructing the line of sight.

A more attractive possibility is that the observed feature is indeed thermal. Though we cannot definitely establish the thermal nature of the emission during the C interval, we wish to remark that the fireball model can account naturally for the presence of these features. In fact, as remarked by both Paczynski (1986) and Goodman (1986) hyper–relativistic expansion naturally leads to the liberation of a fully thermal spectrum, at the time when the fireball expansion becomes optically thin. The initial absence, and later disappearance, of the peak in question does not create difficulties within the fireball model: it can easily be ascribed to inhomogeneities in the time–structure of the relativistic wind, inhomogeneities which are in any case required in order to account for the burst sub–second variability. The fact that the peak, furthermore, appears during the tail of the first pulse of course makes the detection of the weaker thermal component easier (see the very revealing Fig. 2 of Mèszàros and Rees 2000). If this spectral feature is indeed thermal in origin, within the fireball model there is quantitative, and independent check on this identification. In fact, the expected photospheric radius within the fireball model is (Mészáros & Rees 2000) $r_{ph} = 1.2 \times 10^{13} \ cm \ L_{52} Y \eta_2^{-3}$, where L_{52} is the wind luminosity in units of 10^{52} erg s^{-1}, $Y \approx 1$ is the number of electrons per baryon, and η_2 is the flow Lorentz factor η in units of 100. At this radius, the observed photospheric luminosity and temperature are

$L_{ph} = L_{52}(\eta/\eta_\star)^{8/3}$ and $\Theta_{ph} = \Theta_0(\eta/\eta_\star)^{8/3}$, respectively, where $\eta_\star \approx 10^3(L_{52}\mu_1^{-1}Y\Gamma_0)^{1/4}$ and $\Theta_0 = 1236(L_{52}^{1/2}\mu_1^{-1}\Gamma_0^{-1})^{1/2}$ keV, Γ_0 (≥ 1) being the initial bulk Lorentz factor of the wind, and μ_1 the mass, in units of 10 $M_\odot$, of the rotating black hole, from 6 times the gravitational radius of which the fireball is assumed to start its expansion. By fitting simultaneously the observed temperature corrected for the redshift (1.86 keV) and the luminosity of the photosphere ($\sim 2 \times 10^{50}$ erg s^{-1}), we find $\eta \approx 100Y^{1/4}(\mu_1^{-1}\Gamma_0^{11})^{1/54}$ and $L_{52} \approx 2(\mu_1\Gamma_0^{11})^{2/9}$. We thus see that the two independently determined observational parameters, blackbody temperature and luminosity, are well–fitted by values of the theoretical parameters, η and L_{52}, well within the expected range. Assuming unit values for Y, μ_1 and Γ_0, L_{52} results to be about 100 times higher than the estimated 2–700 keV luminosity ($\sim 2 \times 10^{50}$ erg s^{-1}) assuming isotropy. That would imply an efficiency of only 1% in the production of electromagnetic radiation.

In addition to the transient feature, the event shows a spectral evolution that is not typical of other GRBs observed with *BeppoSAX* (Frontera et al. 2000): the peak energy E_p of the $EF(E)$ spectrum (see Table 1 and Figure 3) is constantly above our energy passband for the entire duration of the first pulse, while it takes a low value (~ 10 keV) with the onset of the second pulse. This discontinuity can be the result of two successive electron acceleration episodes, giving rise to the first and the second pulses. The different peak flux behavior of the two pulses with energy, discussed in section 3 confirms this scenario. The emission feature is found only during the first acceleration event.

REFERENCES

Amati, L. *et al.* 2000, Science, 290, 953

Antonelli, L.A. *et al.* 2000, ApJ, 545, L39

Arnaud, K. A. 1996, in ASP Conf. Series 101, Astronomical Data Analysis Software and Systems V, ed. G. H. Jacoby & J. Barnes (San Francisco: ASP), 17

Bakos, G., Sahu, K., Menzies, J., Vreeswijk, P., and Frontera, F. 1999, IAU Circ. No. 7225

Band, D. *et al.* 1993, ApJ, 413, 281

Böttcher, M., Dermer, C.D., Crider, A.W., and Liang, E.P. 1999, A&A, 343, 111

Dal Fiume, D. *et al.* 2000, Adv. Space Res., 25, 399

Dickey, J. M., & Lockman, F.J. 1990, ARA&A, 28, 215

Frontera, F., *et al.* 1997, A&AS, 122, 357

Frontera, F. *et al.* 1999, GCN Circ. 385 (http://gcn.gsfc.nasa.gov/gcn/gcn3/385.gcn3)

Frontera, F. *et al.* 2000, ApJS, 127, 59

Galama, T. *et al.* 1998, Nature, 395, 670

Ghisellini, G. *et al.* 2000, MNRAS, 316, L45

Goodman, J. 1986, ApJ, 308, L47

Heise, J. *et al.* 1999, IAU Circ. 7221

Jager, R., *et al.* 1997, A&AS, 125, 557

Kulkarni, S.R., *et al.* 1998, Nature, 395, 663

Mèszàros, P. and Rees, M.J. 1998, ApJ, 502, L105

Mèszàros, P. and Rees, M.J. 2000, ApJ, 530, 292

Paczyński, B. 1986, ApJ, 308, L43

Pian, E. *et al.* . 2000, ApJ, 536, 778

Piro, L. *et al.* . 1999, ApJ, 514, L77

Piro, L. *et al.* . 2000, Science, 290, 955

Tavani, M. 1996, ApJ, 466, 768

Vietri, M., Ghisellini, G., Lazzati, D., Fiore, F., & Stella, L. 2001, ApJ, in press

Vreeswijk, P.M. *et al.* 2001, ApJ, 546, 672

Yoshida, A. *et al.* 1999, A&AS, 138, 433

Fig. 1.— Light curves of GRB990712 in four energy bands, after background subtraction. The zero abscissa corresponds to 1999 July 12, 16:43:01.6 UT. The time intervals over which the spectral analysis was performed are indicated with vertical dotted lines.

Fig. 2.— Ratio with the Crab count spectrum of the GRB990712 spectra in the time intervals B, C and D, respectively, measured with the WFC No. 2. The Crab spectrum used was measured when this source was observed at an angular offset similar to that of GRB990712.

Fig. 3.— WFC + GRBM spectrum of GRB990712 in the time interval C, along with the best fit curve obtained assuming a power–law plus a blackbody model. *Bottom panel*: ratio between the data and the best fit power–law model alone.

Fig. 4.— $EF(E)$ spectrum of GRB990712 in the time intervals in which we divided the burst time profile (see also Table 1). It is apparent the GRB peculiar spectrum in the interval C.

Table 1.   Spectral evolution of GRB990712 prompt emission

Slice	Duration (s)	Model[a]	$N_{\rm H}$[b]	α	β	E_p(keV)	χ^2/ν
A	4	PL	3.2±2.5	-1.40 ± 0.09		> 700	7.8/6
		PL	[0.0452]	-1.34 ± 0.07			10./7
B	2	PL	2.7±2.1	-1.44 ± 0.08		> 700	4.4/5
		PL	[0.0452]	-1.38 ± 0.06			7/6
C	2	PL	0.3±2.0	-1.66 ± 0.11		> 700	16./6
		PL	[0.0452]	-1.64 ± 0.07			16/7
D	4	PL	[0.0452]	-1.80 ± 0.07		> 700	4.6/6
E	2	PL	[0.0452]	-2.04 ± 0.05			37/7
	2	BL	[0.0452]	-0.4 ± 0.7	-2.4 ± 0.3	11±8	3.5/5
F	3	PL	[0.0452]	-2.01 ± 0.04			89/7
	3	BL	[0.0452]	-0.7 ± 0.4	-2.3 ± 0.2	7±3	4.3/5
G	7	PL	[0.0452]	-2.15 ± 0.05			11/7
	7	BL	[0.0452]	-1.6 ± 0.6	-2.3 ± 0.3	20±15	2.5/5
H	7	PL	[0.0452]	-2.3 ± 0.2			3.0/7

[a]The BL (Band Law) refers to the smoothed broken power-law proposed by Band et al. (1993): α and β are the power–law photon indices below and above the break energy E_0, respectively, and $E_p = E_0(2+\alpha)$ is the peak energy of the $EF(E)$ spectrum.

[b]$N_{\rm H}$ values are given in units of 10^{22} cm^{-2}.

Table 2.   Best fit parameters of the time slice C spectrum

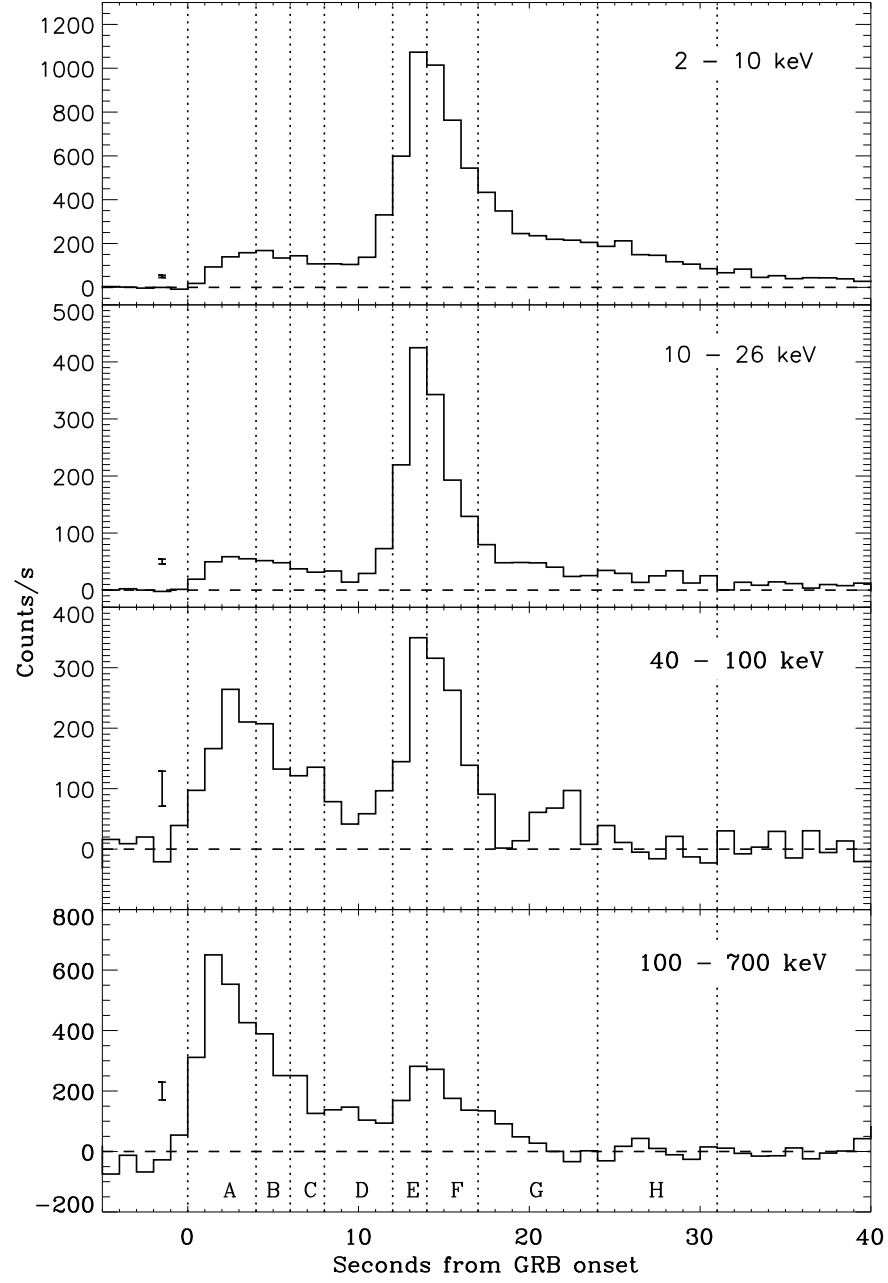| Parameter	PL+Gaussian	PL+BB
α	[1.34]	[1.24]
$F_{\mathrm{PL}}(@1\,\mathrm{keV})$ $[\mathrm{cm}^{-2}\,\mathrm{s}^{-1}]$	1.95 ± 0.24	1.13 ± 0.14
E_{line} [keV]	4.4 ± 0.8	
σ_{line} [keV]	1.4 ± 0.7	
I_{line} $[10^{-8}\ \mathrm{erg\ cm}^{-2}\ \mathrm{s}^{-1}]$	2.7 ± 1.1	
L_{line} $[10^{57}\ \mathrm{phot\ s}^{-1}]$	2.5 ± 0.9	
kT_{bb} [keV]		1.3 ± 0.3
L_{bb} $[10^{49}\ \mathrm{erg\ s}^{-1}]$		2.5 ± 0.6
χ^2/ν	1.6/5	6.2/6

Fig. 1

Fig. 2

Fig. 3

Fig. 4